Stability of the binary colloidal crystals AB_2 and AB_{13}

A. B. Schofield, P. N. Pusey, and P. Radcliffe

Scottish Universities Physics Alliance (SUPA), School of Physics, The University of Edinburgh, Mayfield Road, Edinburgh, EH9 3JZ, United Kingdom

Suspensions of binary mixtures of hard-sphere poly-methylmethacrylate colloidal particles were studied at six different size ratios α. The main aim was to determine the range of size ratios over which the binary colloidal crystals AB_2 and AB_{13} are stable. Combining these results with those of earlier work, we found stability of AB_2 for $0.60 \gtrsim \alpha \gtrsim 0.425$, in good agreement with theoretical predictions by computer simulation and cell model methods. AB_{13} was observed for $0.62 \gtrsim \alpha \gtrsim 0.485$, the lower limit being significantly smaller than the theoretical prediction of about 0.525. Rough measurements of crystallization rates showed that AB_2 tended to crystallize fastest at small size ratios, whereas the opposite was true for AB_{13}. These findings should provide a guide to the optimum conditions for materials applications of these binary colloidal crystals.

I. INTRODUCTION

Assemblies of hard spheres are of interest because they constitute the simplest model for the behavior of fluids, crystals, and glasses, e.g., Ref. [1], and because of the potential to construct functional optical, electrical, and magnetic materials from colloidal precursors which can frequently be well modeled as hard spheres (see Refs. [2,3] for recent examples of such materials applications).

The freezing transition, from a fluid to a crystal, of an assembly of equal-sized hard spheres in thermal motion was discovered in computer simulations [4,5] and confirmed by experiments on colloidal suspensions [6]. Paradoxically, the apparently ordered crystal has a *higher* entropy than the disordered metastable fluid from which it grows. In fact, while the crystal is ordered on the large scale of many lattice spacings, it is locally disordered: spheres in the crystal have more freedom for local motions within the cages formed by their neighbors—resulting in more possible configurations for the system overall—than do spheres in the metastable fluid [7,8].

In a similar vein, mixtures of hard spheres of two different sizes can form ordered binary crystals, again driven by entropy. A useful guideline for candidates for thermodynamically stable binary structures is that they should be "efficient packers" [9]. That is, the total volume fraction ϕ of the crystal when fully compressed should be comparable to, or larger than, the corresponding value, $\phi = \pi/3\sqrt{2} \approx 0.74$, for a one component system. Then, at the lower concentrations where freezing occurs, the particles will have significant local freedom.

Several studies, both theoretical and experimental, of binary hard-sphere crystals have been reported (see Sec. II). The most detailed work so far concerns the structures AB_2 and AB_{13}, where A is the larger sphere. These are found for size ratios $\alpha = R_B/R_A$ between about 0.4 and 0.6 (R denotes radius). The main purpose of this paper is to establish experimentally, more precisely than hitherto, the ranges of size ratio over which the two structures are stable, and to compare the findings with theoretical predictions.

In the next section we review previous work on binary hard-sphere crystals. Section III gives experimental details.

We use colloidal particles of poly-methylmethacrylate, PMMA, now well established as model hard spheres [1]. The main experimental technique used to identify the structures is "powder" light crystallography of the polycrystalline samples. The results are presented in Sec. IV and discussed in Sec. V.

Although, here, we consider only hard-sphere colloids, we mention for completeness that binary crystals of synthetic colloids were found in 1983 by Yoshimura and Hachisu with charged particles that interact through a soft, shielded Coulombic potential [10], and that various binary structures, with possible materials applications, have been observed recently in mixtures of nanometer-sized particles whose interactions were not fully characterized [2,11,12].

II. BACKGROUND

An assembly of equal-sized hard spheres crystallizes into a "random hexagonal close-packed" structure, essentially a random mixture of the two close-packed structures, face-centred cubic and hexagonal close packed [13]. For size ratio α in the range $1 > \alpha \gtrsim 0.85$ concentrated binary hard-sphere mixtures are predicted to form substitutionally disordered crystals, presumably of this same structure, e.g., Ref. [14] and references therein. For $\alpha \lesssim 0.85$, the size difference is too large for both species to readily occupy the same lattice. Then either phase-separated crystals of nearly pure A and nearly pure B or specific ordered binary crystals are expected.

As the size ratio is decreased below 0.85, the first candidate identified so far for an ordered binary hard-sphere crystal is the AB cesium chloride structure, interleaved simple cubic lattices of each species, with one species occupying the body-centred positions in the lattice of the other. This structure has a maximum volume fraction when fully compressed of 0.729 at size ratio $\alpha = \sqrt{3} - 1 = 0.732$, suggesting, by the criterion of Sec. I, that it should not be thermodynamically stable. This expectation was confirmed by more detailed theoretical calculations [15,16]. Experimentally, however, Schofield observed the AB (cesium chloride) structure in

mixtures of PMMA spheres at $\alpha=0.736$ [17], though there were hints that the crystals were metastable. On the other hand, Hunt *et al.* saw no sign of this structure in a similar system at $\alpha=0.72$ [18].

On further decrease of the size ratio, the binary structures AB_2 and/or AB_{13}, which form the main topic of this report (see below), are found in the range $0.62 \gtrsim \alpha \gtrsim 0.42$.

For $\alpha < \sqrt{2}-1=0.414$, the smaller particles are able to fit into the octahedral cavities in a compressed, close-packed structure of the large species. Then the AB sodium chloride structure, interleaved face-centred cubic lattices (or the random-stacked equivalent), is both predicted [19] and observed [18]. In further experimental work at $\alpha < 0.414$, to be reported elsewhere [20], we have found a number of other binary crystals not previously predicted.

Colloidal crystals with the AB_2 and AB_{13} structures were observed by Sanders [21] in a sample of Brazilian gem opal (opals are solidified arrays of spheres of colloidal silica). AB_2 (atomic analogs, borides such as MgB_2) consists of a simple hexagonal arrangement of the A particles with B particles filling the holes between the A layers in a honeycomb structure. In AB_{13} (atomic analogs, UBe_{13} and $NaZn_{13}$) the A particles lie on a simple cubic lattice. Within each cube is a cluster of 13 B particles, a central particle surrounded by 12 others arranged on the vertices of a regular icosahedron. The most efficient packing is obtained when these icosahedral clusters are rotated by 90° between adjacent cubic subcells. This gives a superlattice structure where the unit cell comprises eight subcells and contains 112 particles. Models and sketches of both these structures can be found in, e.g., Refs. [9,22,16]. Murray and Sanders [9] calculated the fully compressed volume fractions for the two structures as functions of the size ratio. For AB_2 they found this to be larger than 0.74 for $0.482 < \alpha < 0.624$, suggesting, by the criterion of Sec. I, thermodynamic stability for this range of size ratios. On the other hand, the fully compressed volume fraction of AB_{13} never exceeds 0.74, but reaches a maximum value close to it of 0.738 at $\alpha=0.558$.

Theoretical calculations of the free energies of AB_2 and AB_{13} have been performed by Eldridge and co-workers [15,19], using Monte Carlo simulations with thermodynamic integration methods, and by Cottin and Monson [16] and Voisey and Bartlett [23] (see also Ref. [18]) using a cell model. Combining these free energies with those predicted by the (accurate) equation of state of Mansoori *et al.* [24] for the binary fluid mixtures allows the equilibrium phase diagrams (see Sec. IV) to be calculated. The predictions of these calculations for the ranges of size ratio within which the two binary structures are thermodynamically stable are summarized in Fig. 1.

Eldridge *et al.* [15] observed stable AB_2 at $\alpha=0.61$ and 0.60. However, in both these cases, it was only found at high concentrations where glass transitions are likely to prevent its experimental observation; thus this region is shown as a dotted line in Fig. 1. AB_2 in coexistence with the binary fluid was first observed at $\alpha=0.59$. At the lower end of the size range, Eldridge *et al.* [19] observed AB_2-fluid coexistence at $\alpha=0.45$ but no sign of AB_2 at $\alpha=0.414$; the dotted line in Fig. 1 indicates the corresponding uncertainty in the lower limit. AB_{13} was observed at high concentration at $\alpha=0.625$
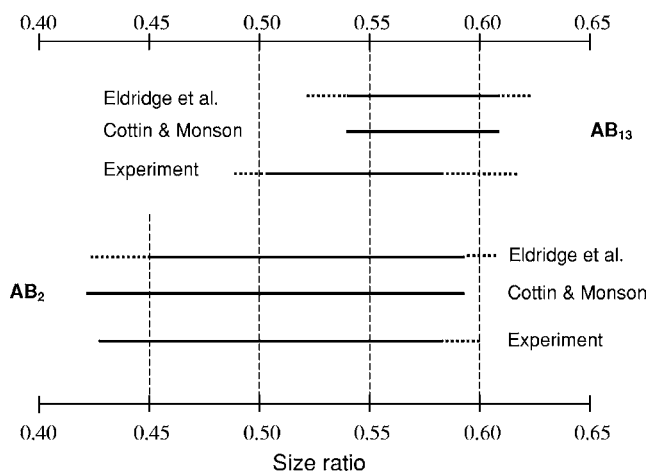

FIG. 1. Comparison of the ranges of stability of the binary hard-sphere crystals AB_2 and AB_{13} predicted by computer simulation (Eldridge *et al.* [15,19]) and cell model theory (Cottin and Monson [16]) with the experimental findings discussed in this paper. The dotted lines indicate uncertainties discussed in the text.

and coexisting with fluid at $\alpha=0.61$ [15]. At the lower end AB_{13} was found to coexist with the fluid at $\alpha=0.54$ but was not seen at all at 0.50 [15].

Cottin and Monson [16] do not show so many phase diagrams, but simply quote the ranges of stability, calculated from their cell model, shown in Fig. 1. Hunt *et al.* [18] also report cell model calculations at $\alpha=0.52$, which did not find AB_{13}, and at $\alpha=0.42$ where neither AB_{13} nor AB_2 were found.

Experimentally, the upper ends of the ranges of stability have been established quite accurately by the work of Bartlett *et al.* on mixtures of PMMA spheres [15,22,25]. At size ratio $\alpha=0.62$ only AB_{13} was observed, and it appeared to be metastable [15,25]. At $\alpha=0.58$, stable AB_2 and AB_{13} were found [22]. Hunt *et al.* [18] also found both structures at $\alpha=0.52$ but neither of them at $\alpha=0.42$ [18]. No other experimental work at the lower ends of the stability ranges has been reported, and this forms the main topic of the remainder of this paper where we study PMMA mixtures with size ratios 0.526, 0.508, 0.487, 0.476, 0.454, and 0.428.

The earlier, similar, study of Hunt *et al.* [18] covered a more widely spaced range of size ratios, 0.72, 0.52, 0.42, and 0.39. The reader is referred to the very full account of this work for further background and other details not given here.

III. EXPERIMENTAL METHODS

A. Sample preparation and characterization

The colloidal particles used in this study were polymethylmethacralate (PMMA) spheres sterically stabilized by chemically grafted poly-(12-hydroxystearic acid). They were prepared by the method of Antl *et al.* [26], and were dispersed in a mixture of decahydronaphthalene (decalin) and tetrahydronaphthalene (tetralin). The proportion of the two liquids were chosen to nearly match the refractive index of the particles, ~ 1.50, providing nearly transparent samples suitable for light scattering.

TABLE I. Data and results for the samples in which AB_2 crystals formed most rapidly at the size ratios indicated; the radii and partial volume fractions of the individual species are listed. The volume fractions of the crystals and their lattice parameters were calculated from the powder diffraction patterns of Fig. 3. The time to crystallize is the elapsed time after the samples were mixed before crystals were first observed. These times are scaled by the relaxation times defined by Eq. (2).

Size ratio α	Radii (nm)	ϕ_A ϕ_B	n_B/n_A	$\phi_{crystal}$	Lattice parameters c & a (nm)	Axial ratio c/a	Axial ratio (theory [34])	Time to crystallize (days)	Relaxation time τ_R (s)	Scaled time ($10^6 \ \tau_R$)
0.526	399	0.257	7.1	0.70	823	0.99	1.04	28	0.89	2.7
	210	0.265			831					
0.508	256	0.330	4.5	0.70	529	1.01	1.02	13	0.24	4.7
	130	0.194			524					
0.487	267	0.268	8.4	0.64	554	0.98	1.02	6	0.27	2.0
	130	0.259			565					
0.476	441	0.433	2.8	0.65	911	0.99	1.02	8	1.20	0.6
	210	0.132			921					
0.454	463	0.476	2.9	0.70	927	0.99	1.00	17	1.39	1.1
	210	0.128			935					
0.428	325	0.421	3.9	0.65	665	1.00				
	139	0.128			667					

The radii of the individual species of PMMA particles were determined by reference to the hard-sphere freezing transition as follows. Stock samples were prepared at a concentration where colloidal fluid and colloidal crystal coexist. They were left to crystallize and phase separate. Powder light crystallography (below) on the crystalline phase gave the wave vector Q_{111} corresponding to the strong reflection from the close-packed planes, the (111) planes for face-centred cubic indexing [13]. From this the lattice parameter a of the crystal was determined via Bragg's law, $Q_{111}a = 2\pi\sqrt{3}$. The volume fraction of the crystal, taken to be the volume fraction at melting, $\phi_M = 0.545$ [5], is given by $\phi_M = (4/a^3)(4\pi R^3/3)$, where we have assumed a face-centred cubic structure with four particles per unit cell. Combination of these two relations gives the following result for the radius R of the particles:

$$R = \frac{\sqrt{3}\pi}{Q_{111}}\left(\frac{3\phi_M}{2\pi}\right)^{1/3} = \frac{3.47}{Q_{111}}. \qquad (1)$$

Because of the large number of particle species involved, we did not systematically measure particle radii by other methods. However, detailed earlier measurements on PMMA spheres in pure decalin [27] and in the decalin-tetralin mixture used here [18] showed good agreement between radii measured by static and dynamic light scattering on dilute suspensions and radii measured by the method used here—crystallography, with the assumption of hard-sphere behavior. This agreement provides further, albeit indirect, evidence that the particles interact like hard spheres.

Sample concentrations were also determined by reference to the hard-sphere freezing transition. Volume fractions of individual stock suspensions, prepared in the fluid-crystal coexistence region, were calculated by assuming that the measured phase volumes follow a lever rule between freezing at

volume fraction $\phi = 0.494$ and melting at $\phi = 0.545$ [5]. Binary mixtures were prepared by mixing appropriate amounts of two stock solutions and diluting, or concentrating by centrifugation, as required. Typically we chose total volume fractions $\phi_A + \phi_B$ between 0.50 and 0.70, where crystallization might be expected, with the ratio by number of small to large particles ranging from less than 2 to more than 13. The samples were mixed thoroughly by slow tumbling.

Individual species of nine different sizes, with radii ranging from 130 to 463 nm, were used in this study. They were mixed in pairs to give six different size ratios, ranging from 0.526 to 0.428. Table I lists the particle sizes and mixtures used.

Because, in these refractive-index-matched samples, the particles are more dense than the mixture of liquids, slow sedimentation of the particles takes place, evident on a time scale of days to weeks. Because formation of the binary crystals often occurs on a similar time scale (see Sec. IV), we may expect that sedimentation can affect the behavior observed. In previous work [18,22,25] these effects were minimized by rotating the samples slowly (once per day) in the vertical plane so that the particles were subjected to "time-averaged zero gravity" [28]. (A few samples have also been studied in the microgravity of space [29].) However, in the work reported here, because so many samples were studied, this was not done. After thorough mixing, the samples were simply left to stand and were observed periodically. Ironically, if one is just interested in whether or not a particular structure can form, this approach has some (accidental) advantage. As sedimentation proceeds, the relative and total concentrations of the two species start to vary with vertical position in the sample. We can expect the total concentration and the relative concentration of larger particles to increase near the bottom of the sample cells, whereas the top becomes depleted in larger particles. Thus a sample which starts with
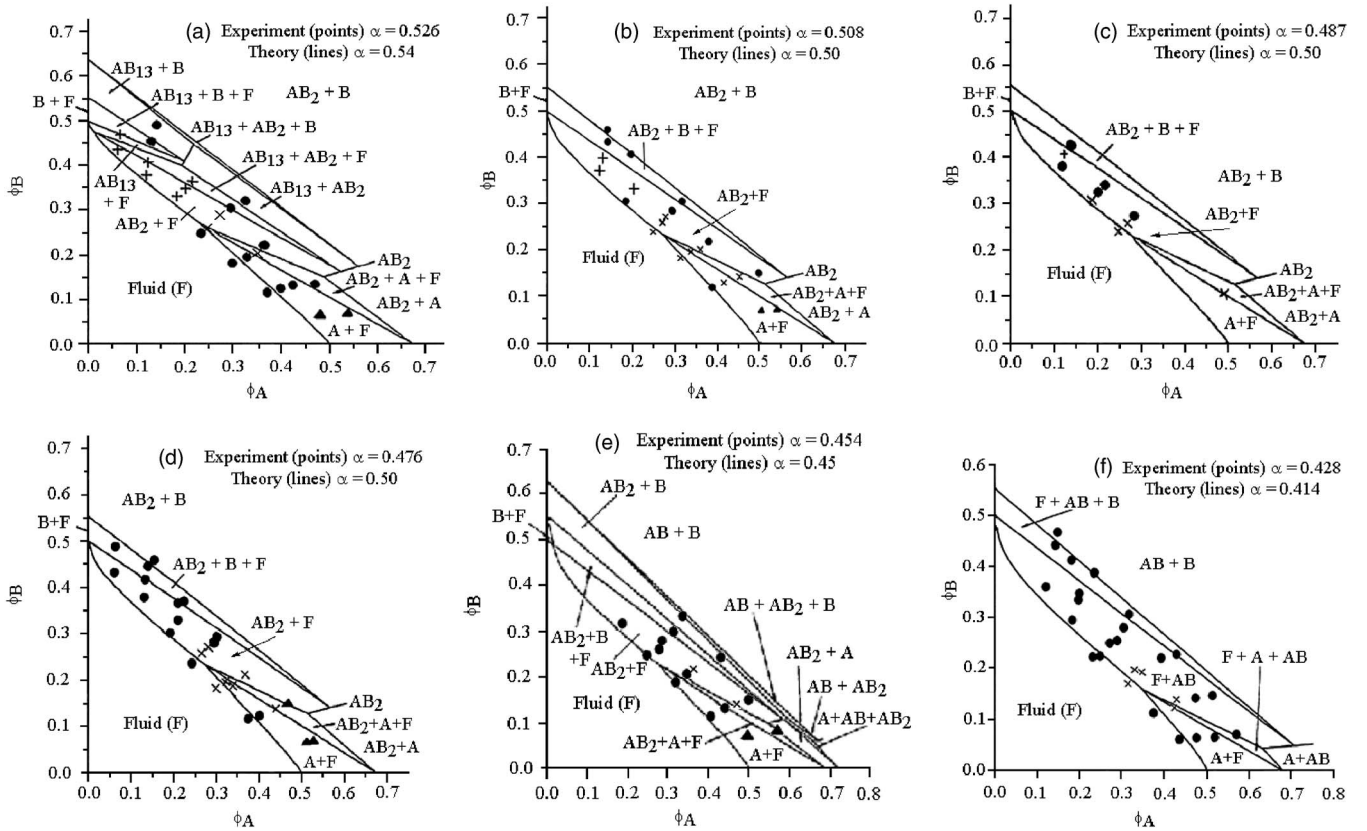
FIG. 2. Theoretical phase diagrams [15,19], as functions of the partial volume fractions ϕ_A and ϕ_B, for binary hard-sphere mixtures at the size ratios α indicated. Regions of predicted two- and three-phase coexistence are shown (A, AB_2, etc. indicate the crystalline phases and F indicates the binary fluid mixture). The symbols indicate the compositions of the samples studied experimentally and the structures observed: solid circle, amorphous; plus sign, AB_{13}; cross, AB_2; triangle, pure A crystal.

particular concentrations ϕ_A and ϕ_B will, in time, "explore" a region of the phase diagram around this initial point, making it more likely that crystallization will occur at some location in the sample (the size ratio, of course, does not change). A disadvantage is that, except for fast-crystallizing species, the phase volumes of, for example, coexisting crystal and fluid cannot be determined accurately. It is also possible that some of the observed binary crystals might be metastable, their formation perhaps being encouraged by a locally sharp gradient in concentration or by a particular history of changing concentrations.

B. Crystallography

Powder light crystallography measurements were performed as described previously [22,30]. The beam from a mixed argon-krypton gas laser was expanded and shaped by an adjustable rectangular aperture of typical dimensions a few millimeters, defining a scattering volume in the sample of similar dimensions. The samples were contained in cylindrical glass cells of internal diameter about 9 mm. These cells were placed on the axis of a cylindrical glass bath of diameter about 8 cm. The bath contained essentially the same mixture of decalin and tetralin as the samples. Because the samples, bath, and glass all had nearly the same refractive index, ~1.50, refraction and reflection of the light at the cell

walls was negligible. The bath acted as a cylindrical lens which imaged the scattered light onto a slit placed at its focus. Behind the slit were placed a diffuser and a photomultiplier detector operating in the photon counting mode. The slit, diffuser, and detector were mounted on an arm which rotated under computer control around the axis of the bath and sample cell. In order to obtain a good average over many crystallites in different orientations, the sample was rotated slowly, about once in two seconds, around its vertical axis during the measurements. The crystallography results are presented in Figs. 3 and 4 as counts per second as a function of scattering vector Q. The scattering vector is given by $Q=(4\pi n/\lambda_0)\sin(\theta/2)$, where n is the refractive index of the sample, λ_0 the wavelength of the light *in vacuo*, and θ is the scattering angle. Most of the data were taken using the Kr$^+$ line, $\lambda_0=647$ nm, or the Ar$^+$ line, $\lambda_0=476$ nm.

IV. RESULTS

A. Phase diagrams

Theoretical phase diagrams for binary hard-sphere mixtures, calculated by Eldridge *et al.* for size ratios $\alpha=0.54$ and 0.50 [15] and $\alpha=0.45$ and 0.414 [19], are shown in Fig. 2. (The cell model phase diagrams reported in Ref. [18] at $\alpha=0.52$ and 0.42 are very similar to those shown in Fig. 2 for $\alpha=0.50$ and 0.414, respectively.) Their topologies have
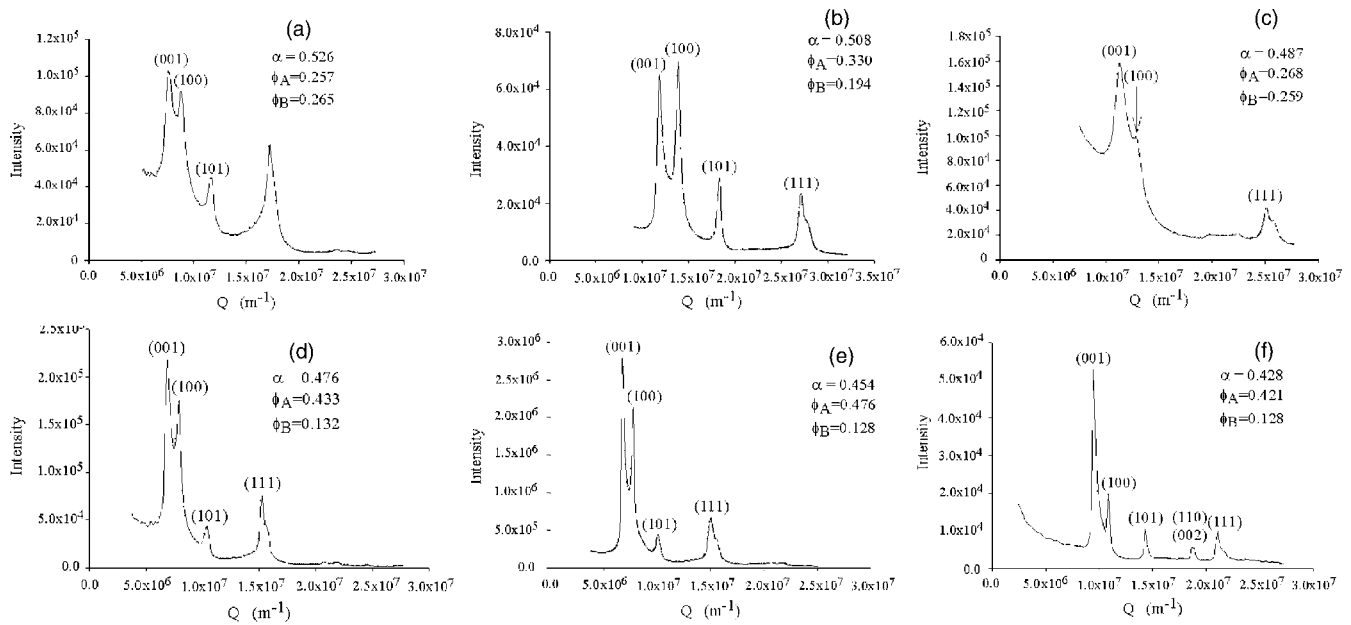
FIG. 3. Crystallography results for the AB_2 binary crystals at the size ratios and compositions indicated; the samples are those, at each size ratio, where crystallization was most rapid. Scattered intensity, in arbitrary units, is plotted against scattering vector.

been discussed elsewhere [15,19]. Briefly, stable fluid is found at concentrations $\phi_A + \phi_B \lesssim 0.50$; on increasing concentration, regions of fluid coexisting with a single crystalline phase, A, AB_2, AB_{13}, or B, are found; at still higher concentrations, two- and three-phase regions, containing various combinations of fluid and the crystalline phases or just the crystalline phases, are predicted.

Also shown in Fig. 2 are the experimental results for size ratios $\alpha = 0.526$, 0.508, 0.487, 0.476, 0.454, and 0.428. The positions of the data points on the diagrams indicate the partial volume fractions, ϕ_A and ϕ_B, of the samples studied, and the symbols indicate the structures (identified by crystallography, Sec. IV B) found. The experimental points are plotted on the theoretical phase diagram with the nearest available size ratio (thus experiment, $\alpha = 0.526$, is compared with theory, $\alpha = 0.54$; experiment, $\alpha = 0.508$, with theory, $\alpha = 0.50$; and so on).

In all cases where crystallization was observed, only one crystal phase was found in any particular sample (or, at least, one structure dominated any others in the diffraction pattern). Although much of the crystallization was observed in regions of the phase diagrams where crystal-fluid coexistence is predicted, we did not, for the reasons given is Sec. III A, make a detailed study of phase coexistence. Thus the symbols in Fig. 2 simply indicate the crystal structure found, or, in the case of no crystallization, an amorphous mixture.

At $\alpha = 0.526$ [Fig. 2(a)], AB_{13} was found in several samples. These are broadly in the region of the phase diagram predicted, but detailed agreement with theory is not observed. Samples showing AB_2 crystallization were found in regions where AB_2 is predicted. Interestingly, however, samples with the stoichiometry two B's to one A [indicated by extrapolation of the line labeled AB_2 in Fig. 2(a) towards the origin] did not crystallize but remained amorphous over several weeks of observation. These findings, for both AB_{13}

and AB_2, are broadly similar to the results of Hunt *et al.* [18] at $\alpha = 0.52$. They are also similar to previous findings at $\alpha = 0.58$ [15]; this paper can be consulted for more complete discussion of the comparison between experiment and theory.

Theory predicts that AB_{13} should no longer be stable at $\alpha = 0.50$ (Fig. 1). However, Fig. 2(b) shows that, at $\alpha = 0.508$, several samples crystallized into AB_{13} at roughly the stoichiometry of 13 B's to one A. At this size ratio, AB_2 was observed mainly in regions where it is predicted, including two samples not far from the stoichiometry of two B's to one A.

At $\alpha = 0.487$ [Fig. 2(c)], one sample showed AB_{13} crystals. As predicted, AB_2 was observed over a quite wide region of the phase diagram at this size ratio.

For $\alpha \lesssim 0.476$, AB_{13} was no longer found, though AB_2 was observed, as predicted, at $\alpha = 0.476$ [Fig. 2(d)] and 0.454 [Fig. 2(e)]. Theory predicts no AB_2 at $\alpha = 0.414$, but a significant region of AB_2 was found experimentally at $\alpha = 0.428$ [Fig. 2(f)]. By contrast, Hunt *et al.* [18] did not find AB_2 at $\alpha = 0.42$.

A notable general feature of Fig. 2, observed also in previous work [15,18,22,25], is the large number of samples that do not show the predicted crystallization behavior but that remain in amorphous, presumably nonequilibrium, states over the period of observation [31]. Binary mixtures appear to display a complex pattern of glass formation which could be further investigated by dynamic light scattering, as for one-component systems [32].

B. Crystallography

The equipment used for the crystallography measurements was described in Sec. III B. Crystalline samples typically contained many small crystallites in random orientations and, superficially, looked similar to one-component
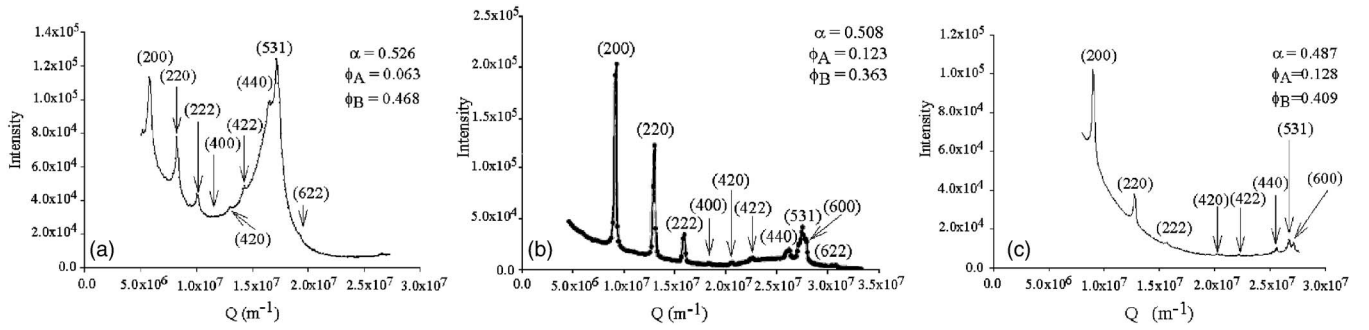
FIG. 4. Crystallography traces for the AB_{13} binary crystals.

systems [6]. Often, crystallites were only observed in a limited region at some height in the sample. In these cases, the beam-shaping aperture was adjusted so that only the crystalline region was illuminated.

In Fig. 3 (AB_2) and Fig. 4 (AB_{13}) we show typical powder patterns for each size ratio. Analysis of the patterns is summarized in Tables I and II. After mixing, the samples were observed periodically and, in most cases, the elapsed time after which crystals were first observed was noted. The crystallography results shown in Figs. 3 and 4 are for the samples at each size ratio which crystallized soonest. The partial volume fractions, ϕ_A and ϕ_B, of these samples are given in Tables I and II, allowing one to identify the samples in Fig. 2. The corresponding times to crystallize are also listed in Tables I and II.

In order to be able to compare the crystallization times for particles of different sizes, we need to scale them by a relaxation time that describes the rate of particle diffusion in the sample (assuming that nucleation and growth of the crystals are controlled by diffusion). An obvious definition for such a relaxation time is

$$\tau_R = \frac{R_A^2}{D}, \qquad (2)$$

where R_A is the radius of the larger particle and D is its long-time self diffusion constant; τ_R is then roughly the time that it takes a large particle to diffuse a distance equal to its own diameter. The problem with this definition is that the magnitude of the long-time self-diffusion coefficient in concentrated binary mixtures is not known, and even in one-

component systems it depends strongly on concentration [33]. Thus we take D to be the "bare" diffusion constant which applies to a dilute suspension,

$$D = \frac{k_B T}{6 \pi \eta R_A}; \qquad (3)$$

$k_B T$ is the thermal energy and η is the viscosity of the solvent, taken here to be 3×10^{-3} Pa for the mixture of decalin and tetralin. This is a well-defined procedure, but it should be borne in mind that it underestimates the actual relaxation time of the concentrated system by a factor of 100 or more [33].

1. AB_2

The diffraction patterns shown in Fig. 3 are consistent with the simple hexagonal structure of AB_2. Consider Fig. 3(b) as an example. From the position of the first line, (001), we calculate the lattice parameter c which gives the spacing of the planes along the hexagonal axis. The second line, (100) or (010), gives the lattice parameter a, the in-plane spacing of the A particles. The third line observed is (101), (011). The fourth line, at $Q = 2.71 \times 10^7$ m^{-1}, is (111) and the shoulder at slightly higher scattering vector comprises (200) and (102) [and (020) and (012)]. The lines (110) and (002), which are expected to lie between (101) and (111) are not observed in Figs. 3(a)–3(e), probably due to minima in the particles' form factors, but are apparent in Fig. 3(f).

From the lattice parameters of the crystals, calculated from the powder patterns of Fig. 3, one can calculate the

TABLE II. Data and results for the AB_{13} crystals. See caption to Table I for details.

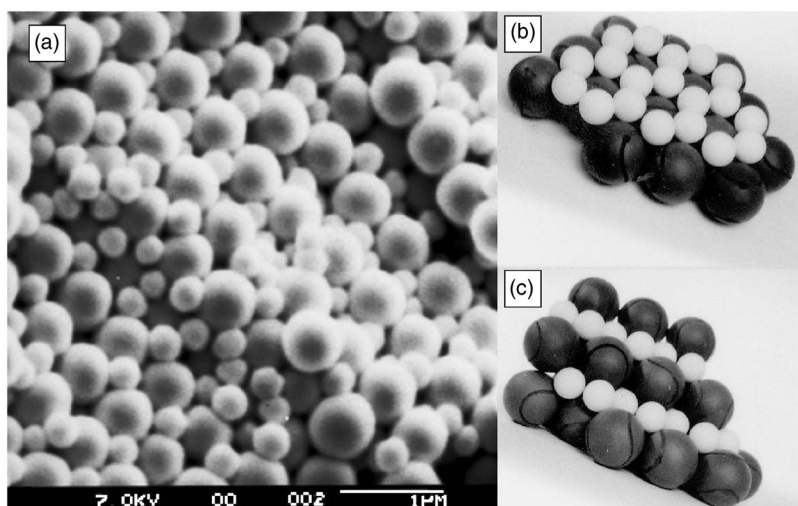| Size ratio α	Radii (nm)	ϕ_A ϕ_B	$\phi_{crystal}$	Time to crystallize (days)	Relaxation time τ_R (s)	Scaled time ($10^6 \ \tau_R$)
0.526	399	0.063	0.61	11	0.89	1.1
	210	0.468				
0.508	256	0.130	0.61	9	0.24	3.2
	130	0.363				
0.487	267	0.130	0.60			
	130	0.409				

FIG. 5. Scanning electron micrograph of an AB_2 crystal at size ratio $\alpha=0.428$ ($\phi_A=0.421$, $\phi_B=0.128$). Mainly the (011) plane is seen, with steps at the upper right and lower left. The left-hand step exposes a portion of the (001) plane on which the hexagonal honeycomb arrangement of the small particles can be seen. The models in (b) and (c) show the AB_2 crystal (100) and (001) planes and can be used for comparisson with the electron micrograph.

total volume fractions of the crystals, $\phi_{\text{crystal}}=\phi_A+\phi_B$, listed in Table I. The calculated volume fractions range from 0.64 to 0.70, showing no apparent trend with size ratio (Table I). These values can be compared to the smallest crystal volume fraction predicted theoretically of ~0.645 (Fig. 2). Note that the experimental volume fractions are calculated from the radii of the particles and the two lattice parameters of the crystal. All four of these quantities are derived from crystallography measurements (Sec. III A), so are susceptible to errors arising from any misalignment of the scattering equipment. We estimate that the uncertainty in the crystal volume fraction is of order ±0.02.

The axial ratios of the observed crystals lie in the range $c/a=1.00\pm0.02$ (Table I), with an estimated uncertainty of about ±0.02. These values can be compared with the theoretical predictions of Eldridge *et al.* [34], also listed in Table I, for strain-free AB_2 crystals at the corresponding volume fractions and size ratios. For the smaller size ratios, $\alpha=0.508-0.428$, there is reasonable agreement between experiment and theory, with c/a close to 1 in both cases. However, the value, $c/a=0.99\pm0.02$, found at $\alpha=0.526$ is significantly smaller than both the theoretical prediction, $c/a=1.04$, and the value, also 1.04, found experimentally by Hunt *et al.* [18] at $\alpha=0.52$. It is possible that our crystals were distorted by gravity, an effect not expected in the experiments of Hunt *et al.* who used the "time-averaged zero gravity" method mentioned in Sec. III A. However, it is then not clear why the samples at smaller size ratio were not similarly affected.

As shown in Table I, the crystallization times are typically of order one million relaxation times. (Note that these are "bare" relaxation times applying to dilute systems. As discussed above, the relaxation time describing diffusion in the concentrated system of interest is probably at least 100 times larger, so that the crystallization times are of order 10 000 "dressed" relaxation times.) By contrast, fastest crystallization times for one-component systems are around one thousand relaxation times (a few minutes) [35]. Not surprisingly, the nucleation process in a binary suspension, involving ordered segregation of the two species, is much slower and, presumably, more complicated than that in a one-component system. There is a slight trend towards faster crystallization

as the size ratio is decreased (see also Sec. V), perhaps reflecting the increasing ease with which the smaller particles can be incorporated into the lattice.

2. AB_{13}

The reflections labeled with even Miller indices for AB_{13} (Fig. 4 and Table II) correspond to a simple cubic lattice [for which the indices would be (100), (110), (111), etc.]. The observation of superlattice lines with odd indices—of which (531) is, as in previous work [22,25], the strongest—confirms that the structure is indeed AB_{13}. As described in Sec. II, the unit cell of AB_{13} consists of eight simple cubic subcells containing icosahedra of B particles which are rotated by 90° between adjacent cubic subcells. The lattice parameter is double that of a subcell, leading to doubling of the cubic Miller indices.

The calculated volume fractions of the crystal, $\phi_{\text{crystal}}=0.60-0.61$, are similar to the smallest value ~0.60 predicted theoretically by the phase diagram at $\alpha=0.54$ [Fig. 2(a)].

The scaled crystallization times (Table II), of order one million relaxation times, are similar in magnitude to those observed for AB_2 (Table I). Accidentally, the sample at $\alpha=0.487$ that showed AB_{13} crystals was not monitored regularly; it was neglected for several months after which time the crystals were discovered in a band in the middle of the sample. Thus we do not have a reliable crystallization time for this sample.

C. Electron microscopy

Another way to study the structure of hard-sphere colloidal crystals is by scanning electron microscopy. Crystalline samples are allowed to dry slowly; the dry compacted solid is cleaved and gold coated by sputtering. We show two examples which display features not previously published.

Dried crystals of AB_2 tend to cleave along the (011) plane; Ref. [22] shows such a picture with a large ordered region displaying interleaved lines of large and small particles. Figure 5 shows a similar image (sample at $\alpha=0.428$, $\phi_A=0.421$, $\phi_B=0.128$) except that steps are seen on the (011)
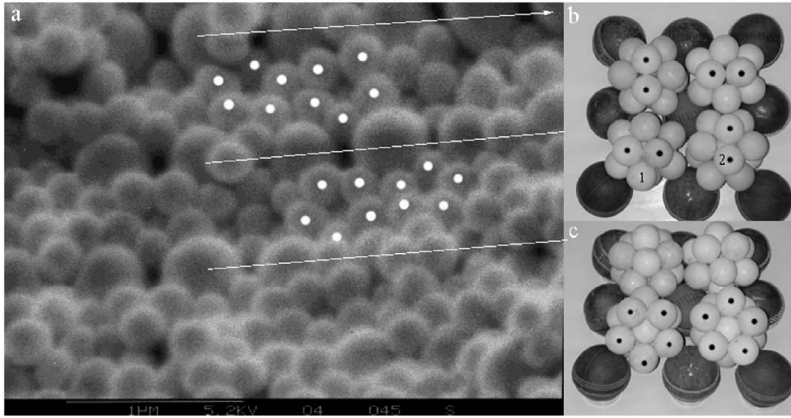
FIG. 6. Scanning electron micrograph of an AB_{13} crystal ($\alpha=0.508$, $\phi_A=0.130$, $\phi_B=0.392$). Parallel lines indicate rows of large particles in the (011) plane. Pentagons (indicated by dotted spheres), resulting from the removal of one small particle from each of the icosahedral clusters, can be seen between the rows. At the top center and center, the different orientations of adjacent icosahedra are evident. The model in (b) shows the AB_{13} superlattice (100) plane and the orientation of the icosahedra. Removal of spheres 1 and 2 reveal the underlying pentagons as shown in (c).

plane. The left-hand step exposes a section of the (001) plane on which the honeycomb structure of the small B particles can be seen.

For AB_{13}, the drying process tends to disrupt the crystal, though some order remains [22]. (Note, however, that the powder patterns of Fig. 4 indicate a high degree of order in the wet samples.) Figure 6 shows an electron microscope image of an AB_{13} sample at size ratio $\alpha=0.508$ ($\phi_A=0.130$, $\phi_B=0.392$). Roughly, the (011) plane is exposed. The parallel lines mark rows of large A particles. Dots indicate pentagons of small particles resulting from icosahedral clusters from which one particle has been removed. At the top of the picture, and at the left, the different orientations of adjacent icosahedra (pentagons) are clearly evident. (A similar, but less structured, picture was shown in Ref. [22].)

V. DISCUSSION

The ranges of size ratio α over the AB_2 and AB_{13} binary hard-sphere crystals are predicted theoretically to be stable were discussed in Sec. II and are summarized in Fig. 1. There we also described the experimental situation at the upper end of the range.

In the present work, AB_2 was observed at the smallest size ratio studied, $\alpha=0.428$ (Sec. IV A). However, Hunt *et al.* [18] did not find AB_2 at $\alpha=0.42$, and, in work to be reported elsewhere [20], we did not observe it at $\alpha\approx0.41$. These results provide an experimental lower limit for the stability of AB_2 of $\alpha\approx0.425$. As shown in Fig. 1, this is in good agreement with the predictions of the cell model calculations (Cottin and Monson) and not in disagreement with the computer simulations of Eldridge *et al.*

We observed AB_{13}, at roughly the stoichiometry of 13 B's to one A, in several samples at size ratio $\alpha=0.508$ and also in one sample at $\alpha=0.487$ (Sec. IV A). However, no AB_{13} was observed at $\alpha=0.476$. Thus we can take $\alpha\approx0.480$ as the experimental lower limit for stability of AB_{13}. However, since it is possible that, for the reasons given in Sec. III, the one crystal observed at $\alpha=0.487$ may be metastable, we indicate the region between $\alpha=0.480$ and 0.508 by a dashed line in Fig. 1. Nevertheless, it is clear from Fig. 1 that the experimentally observed lower limit, $\alpha=0.48-0.50$, for the stability of AB_{13} is significantly smaller than that, $\alpha=0.52-0.54$, predicted by theory.

There are several possible reasons why theory and experiment may disagree. First, there is inevitably some uncertainty in the theoretical predictions associated, for example, with approximations inherent in the cell model approach and possible inaccuracy of the fluid equation of state of Mansoori *et al.* [24]. Second, the individual species of particles used in the experiments, in common with all colloids, have some distribution of particle size or polydispersity. Typically, for our particles, the standard deviation of the size distribution divided by its mean was about 0.05. Even polydispersities as small as this have been shown to affect significantly both the phase behavior, e.g., Ref. [36], and the crystallization kinetics [37] of one-component systems. However, without much more work, it would be difficult to elucidate the precise influence of polydispersity on binary systems.

Another experimental uncertainty which has emerged recently is the finding that the PMMA spheres, long thought to be uncharged in nonpolar liquids and to interact like hard spheres, can, under some conditions, carry a significant charge [38,39]. Charging appears to be most evident when fluorescently labeled particles are suspended in a liquid mix-

TABLE III. Compilation of scaled crystallization times for AB_2 and AB_{13} crystals at various size ratios, taken from references indicated. The Comment column indicates the gravitational conditions under which the experiments were performed; slow rotation refers to the time-averaged zero-gravity conditions described in Sec. III A.

Size ratio α	Ref.	Comment	AB_2 Scaled time ($10^6 \, \tau_R$)	AB_{13} Scaled time ($10^6 \, \tau_R$)
0.58	[22]	Slow rotation	20	2.3
0.57	[28]	Space, microgravity		0.35
0.52	[18]	Slow rotation	17	25
0.526	this work	Normal gravity	2.7	1.1
0.508	this work	Normal gravity	4.7	3.2
0.487	this work	Normal gravity	2.0	
0.476	this work	Normal gravity	0.6	
0.454	this work	Normal gravity	1.1	
0.428	this work	Normal gravity		

ture containing bromo-cycloheptane to match their density, or when surfactant or salt are added to the suspension. None of these conditions applied in the present work, but the possibility that the interaction between the particles may be slightly affected by charge, which in turn could affect both phase behavior [40] and crystallization kinetics [41], cannot be completely discounted. There appears to be no information in the literature on charge in the PMMA-decalin-tetralin system, and we did not attempt to measure it ourselves.

In Table III we compare our observations of crystallization rates with those of other work. First we note that these are not precise measurements, but rather rough estimates of the time to see the first crystals made by different observers. Nevertheless some qualitative conclusions can be drawn. Most striking is the difference of around a factor of 10 between the crystallization rates observed by Hunt *et al.* [18] at $\alpha=0.52$ and our findings at $\alpha=0.526$. It appears that, while the slow rotation (see Sec. III A) of the samples used by Hunt *et al.* is effective in preventing separation of the two species by sedimentation, it does strongly suppress crystallization compared to samples studied under normal gravity. Presumably the slow flow in the samples caused by the ro-

tation disrupts nucleation. Also striking is the fact that the one sample studied in space, AB_{13} at $\alpha=0.57$, is the fastest crystallizer of all. We must conclude that even slow differential sedimentation under normal gravity is enough to retard nucleation noticeably. However, if we discount the results of Hunt *et al.* and recognize that the crystallization time found for AB_{13} at $\alpha=0.58$ is also large because of slow rotation of the sample, there is a suggestion from Table III that AB_{13} crystallizes more quickly at the larger size ratios. On the other hand, for AB_2 the trend appears to be for faster crystallization at the smaller size ratios. While these may be useful observations for guiding materials applications, at this stage we do not have enough information to speculate on the underlying microscopic mechanisms.

[1] P. N. Pusey, in *Liquids, Freezing and Glass Transition*, edited by J. P. Hansen, D. Levesque, and J. Zinn-Justin (North-Holland, Amsterdam, 1991), pp. 763–942; V. J. Anderson and H. N. W. Lekkerkerker, Nature (London) **416**, 811 (2002).

[2] F. X. Redl, K. S. Cho, C. B. Murray, and S. O'Brien, Nature (London) **423**, 968 (2003).

[3] J. Kalkman, E. de Bres, A. Polman, Y. Jun, D. J. Norris, D. C. 't Hart, J. P. Hoogenboom, and A. van Blaaderen, J. Appl. Phys. **95**, 2297 (2004).

[4] B. J. Alder and T. E. Wainwright, J. Chem. Phys. **27**, 1208 (1957).

[5] W. G. Hoover and F. H. Ree, J. Chem. Phys. **49**, 3609 (1968).

[6] P. N. Pusey and W. van Megen, Nature (London) **320**, 340 (1986).

[7] D. Frenkel, Phys. World **6** (2), 24 (1993).

[8] B. J. Ackerson, Nature (London) **365**, 11 (1993).

[9] M. J. Murray and J. V. Sanders, Philos. Mag. A **42**, 721 (1980).

[10] S. Yoshimura and S. Hachisu, Prog. Colloid Polym. Sci. **68**, 59 (1983); J. Phys. (Paris), Colloq. **46**, C3-115 (1985).

[11] E. V. Shevchenko, D. V. Talapin, A. L. Rogach, A. Kornowski, M. Haase, and H. Weller, J. Am. Chem. Soc. **124**, 11480 (2002).

[12] A. E. Saunders and B. A. Korgel, ChemPhysChem **6**, 61 (2005).

[13] P. N. Pusey, W. van Megen, P. Bartlett, B. J. Ackerson, J. G. Rarity, and S. M. Underwood, Phys. Rev. Lett. **63**, 2753 (1989).

[14] W. G. T. Kranendonk and D. Frenkel, Mol. Phys. **72**, 679 (1991).

[15] M. D. Eldridge, P. A. Madden, P. N. Pusey, and P. Bartlett, Mol. Phys. **84**, 395 (1995).

[16] X. Cottin and P. A. Monson, J. Chem. Phys. **102**, 3354 (1995).

[17] A. B. Schofield, Phys. Rev. E **64**, 051403 (2001).

[18] N. Hunt, R. Jardine, and P. Bartlett, Phys. Rev. E **62**, 900 (2000).

[19] E. Trizac, M. D. Eldridge, and P. A. Madden, Mol. Phys. **90**, 675 (1997).

[20] A. B. Schofield and P. N. Pusey (unpublished).

[21] J. V. Sanders, Philos. Mag. A **42**, 705 (1980).

[22] P. Bartlett, R. H. Ottewill, and P. N. Pusey, Phys. Rev. Lett. **68**, 3801 (1992).

[23] J. P. Voisey and P. Bartlett (unpublished).

[24] G. A. Mansoori, N. F. Carnahan, K. E. Starling, and T. W. Leland, J. Chem. Phys. **54**, 1523 (1971).

[25] P. Bartlett, R. H. Ottewill, and P. N. Pusey, J. Chem. Phys. **93**, 1299 (1990).

[26] L. Antl, J. W. Goodwin, R. D. Hill, R. H. Ottewill, S. M. Owens, S. Papworth, and J. A. Waters, Colloids Surf. **17**, 67 (1986).

[27] P. N. Segrè, O. P. Behrend, and P. N. Pusey, Phys. Rev. E **52**, 5070 (1995).

[28] P. Bartlett, P. N. Pusey and R. H. Ottewill, Langmuir **7**, 213 (1991).

[29] R. J. Christianson *et al.* (unpublished).

[30] V. C. Martelozzo, A. B. Schofield, W. C. K. Poon, and P. N. Pusey, Phys. Rev. E **66**, 021408 (2002).

[31] We note that, when left for several months, some of the samples marked as amorphous in Fig. 2 did display thin layers of pure *B* crystal at the top as a result of preferential removal by sedimentation of the larger *A* particles, followed by sedimentational compression of the remaining *B* particles.

[32] W. van Megen and S. M. Underwood, Phys. Rev. E **49**, 4206 (1994).

[33] W. van Megen, T. C. Mortensen, S. R. Williams, and J. Muller, Phys. Rev. E **58**, 6073 (1998).

[34] M. D. Eldridge, P. A. Madden and D. Frenkel, Mol. Phys. **80**, 987 (1993).

[35] J. L. Harland and W. van Megen, Phys. Rev. E **55**, 3054 (1997).

[36] M. Fasolo and P. Sollich, Phys. Rev. E **70**, 041410 (2004).

[37] S. Martin, G. Bryant, and W. van Megen, Phys. Rev. E **67**, 061405 (2003); **71**, 021404 (2005).

[38] A. Yethiraj and A. van Blaaderen, Nature (London) **421**, 513 (2003).

[39] M. F. Hsu, E. R. Dufresne, and D. A. Weitz, Langmuir **21**, 4881 (2005).

[40] A. P. Hynninen and M. Dijkstra, Phys. Rev. E **68**, 021407 (2003).

[41] S. Auer and D. Frenkel, J. Phys.: Condens. Matter **14**, 7667 (2002).